Land Cover Change and Its Effects on Catchment Hydrology: A Quantitative Analysis Using SWAT in Horní Úpa

Nikol Zelíková[1,2], Markéta Potůčková[4], Marek Purm[1,3], Václav Šípek[1*], Kristýna Falátková[1], Michael Hofbauer[1,2], Alex Šrollerů[4], Lucie Červená[4], Zuzana Lhotáková[5], Jana Albrechtová[5], Lucie Kupková[4]

[1] Institute of Hydrodynamics of the Czech Academy of Sciences, Pod Paťankou 30/5, Prague, 160 00, Czechia
[2] Department of Water Resources and Environmental Modelling, Faculty of Environmental Sciences, Czech University of Life Sciences Prague, Kamýcká 129, Praha-Suchdol, 165 00, Czechia
[3] Department of Physical Geography and Geoecology, Faculty of Science, Charles University in Prague, Albertov 6, Prague, 120 00, Czechia
[4] Department of Applied Geoinformatics and Cartography, Faculty of Science, Charles University in Prague, Albertov 6, Prague, 120 00, Czechia
[5] Department of Experimental Plant Biology, Faculty of Science, Charles University in Prague, Albertov 6, Prague, 120 00, Czechia

*Corresponding author: sipek@ih.cas.cz

Abstract

The changes in land cover, particularly in vegetation, directly influence the regional water systems through various processes and have potential to alter not only microclimates and local hydrological regimes, but also local ecosystems and downstream water resources. This study investigates the interplay between land cover change and hydrological processes over a 30-year period in the mid-latitude mountainous catchment. Key vegetation trends were identified by supervised classification of geometrically and radiometrically corrected Landsat satellite imagery. Specifically, the replacement of coniferous forests with transitional woodland-shrub and a gradual increase in mixed forests, influenced by disturbance events such as windthrows and bark beetle outbreaks, were observed. The SWAT model was successfully calibrated and validated using long-term discharge data, allowing for the simulation of land cover scenarios. Results suggest that land cover changes exerted rather limited influence on total water balance, indicating a certain degree of hydrological resilience of the catchment. However, they affected the partitioning of runoff components, such as direct flow, subsurface lateral flow and groundwater recharge. The study demonstrates the value of integrating satellite-based land cover analysis with process-based modelling to understand long-term land-hydrology interactions in complex terrain. The findings underscore the importance of improving spatial resolution, dynamic vegetation modelling, and soil-vegetation parameterization for future assessments under changing environmental conditions. This research contributes to a growing body of knowledge essential for sustainable water resource management in sensitive mountain regions.

Key words: land cove change, hydrological modelling, SWAT model, Landsat

1. Introduction

In the last six decades, land cover change concerned about one-third of the global land area (Winkler et al. 2021). The changes in land cover, particularly in vegetation, directly influence the regional water systems through various processes, such as evapotranspiration, interception or infiltration (Wang et al. 2018; Chen et al. 2021). This is caused by the role of vegetation as an interface between the soil and the atmosphere (Dubbert and Werner 2018). These alterations in the hydrological cycle have also profound effects on the surface energy balance, carbon cycle and land surface-atmosphere interactions, influencing air temperature and precipitation patterns, humidity levels, and surface's albedo (Meier et al. 2021; Perugini et al. 2017). They have potential to alter not only microclimates and local hydrological regimes, but also local ecosystems and downstream water resources.

A wide range of remote sensing and GIS-based techniques are used to analyze land cover change, enabling the assessment of spatial and temporal dynamics in vegetation cover (Feranec et al. 2014, 2016; Ramon et al. 2020; Kupková et al. 2021, 2023). One of the most common approaches is the classification of multi-temporal satellite imagery, such as Landsat or Sentinel-2, which allows for the detection of land cover transitions over decades (Kupková et al. 2018, Chaves et al. 2020). Change detection methods, including supervised classification, vegetation indices (e.g., NDVI, EVI, DI, forest z-score), and machine learning algorithms, are commonly applied to quantify deforestation, afforestation, or shifts in vegetation structure (Haeley et al. 2005, Huang et al. 2010, Talukdar et al. 2020, Gao et al. 2020).

As land cover affects the hydrological cycle in numerous ways, it is vital to analyze the land coverage by particular vegetation types. Forested areas use significant amount of water for transpiration (Jasechko et al. 2013; Sutanto et al. 2014) and a notable part of precipitation is not reaching the soil surface due to interception (Kofroňová et al. 2021). Infiltration from precipitation is in the forest also increased due to root growth and organic matter, enhancing the soil's ability to absorb and retain water (Alaoui et al. 2011; Archer et al. 2015) compared to urban or agricultural lands, affecting the flow regimes of rivers and streams (Yang et al. 2011). In contrast, meadows and urban areas have markedly different impacts on the hydrological cycle. Meadows, with their lower vegetation height and density, tend to have higher surface runoff (Blackburn et al. 2021) and less transpiration compared to forests (Pielke et al. 1998). Water table height in montane meadows determines their potential to be a large carbon sequestration sink in the context of changing hydroclimates and different land management decisions impacting meadow hydrology (Blackburn et al. 2021). Agricultural or urban areas, characterized by less permeable or impervious surfaces, dramatically reduce

infiltration and increase surface runoff, leading to higher peak flows in urban streams and rivers (Sieker 2000; Blöschl 2022).

To predict the effects of land cover changes on the hydrological regime, hydrological models serve as valuable tools for managing water resources more effectively (Mensah et al. 2022). Numerous studies have utilized hydrological models to simulate the impacts of deforestation (Danáčová et al. 2020), afforestation (Sonnenborg et al. 2017), urbanization (Trinh and Chui 2013), and other land cover changes on various components of the hydrological cycle, such as stream flow (Cognard-Plancq et al. 2001), evapotranspiration (Launiainen et al. 2019), and groundwater recharge (Sonnenborg et al. 2017). However, the correct representation and parametrization of land cover in hydrological models is crucial for predicting hydrological responses to environmental changes. Inaccurate representation of land cover can lead to significant errors in model outputs (Yu et al. 2016).

In this study, we therefore combine a detailed analysis of landcover change over 30 years with a modelled catchment water balance. The selected study area is a forested mountain basin in the Krkonoše Mountains, Czechia. Our goal is to contribute to the understanding of the complex interactions between land use changes and the hydrological cycle. The specific aims of this study are: (1) quantification of land cover change in mid-latitude mountainous catchment over 30 years, (2) correct representation of the catchment water balance using a semi-distributed model, and (3) assessing the influence of time-varying land cover on the hydrological response, including two scenarios - afforestation and deforestation of the catchment.

2. Experimental area and methods

2.1 Experimental area

The Horní Úpa catchment is situated in the headwaters of the Krkonoše Mountains in the Czechia, Central Europe, covering an area of 82 km² (Fig. 1). The experimental area is a part of the KRNAP National Park. The altitude ranges from 600 to 1,600 meters above sea level. The region is part of the Lugicum unit of the Bohemian Massif and is primarily composed of metamorphic gneisses and schists with granite intrusions. Hydrogeologically, it is classified as a hard rock system (Lachassagne et al. 2011). The area is predominantly covered by shallow soils, namely crypto-podzols, podzols, rankers or cambisols. Forests and transitional forest zones dominate over 80% of the catchment, with coniferous species, particularly spruce, comprising 89% of the forest cover.

According to the Köppen climate classification, the catchment falls within the subarctic (Dfc) climate zone, with coldest month below 0 °C and 1–3 months averaging above 10 °C characterized by warm summers and relatively evenly distributed precipitation (Tolasz 2007).

From 1990 to 2023, observations at the Pec pod Sněžkou meteorological station recorded an average annual air temperature of 5.4 °C and an average annual rainfall of 1,319 mm. The annual runoff height from the catchment is approximately 920 mm, representing ~70% of the total precipitation.

2.2 Land cover data

A 30-year time series of land cover in the Horní Úpa catchment was derived by supervised classification of geometrically and radiometrically corrected Landsat satellite imagery (L2 processing level, surface reflectance) acquired by the Thematic Mapper (TM), Enhanced Thematic Mapper + (ETM+) and Operational Land Imager (OLI) sensors. Due to the frequent occurrence of cloud cover in this area, cloud-free mosaics were first created by setting an optimized percentile of the valid pixel values of all available imagery within each growing season (day of year (DOY) 150–270). The quality band of the L2 product was used to select invalid pixels, i.e., pixels with cloud cover or obscured by cloud cover, pixels out of radiometer range, etc. (Zhu and Woodcock 2014). Years in which it was not possible to derive a cloud-free mosaic were omitted or replaced by a two- or three-year composite if the gap was greater than one year. For the given period 1991 to 2022, 23 datasets were created (Table 1).

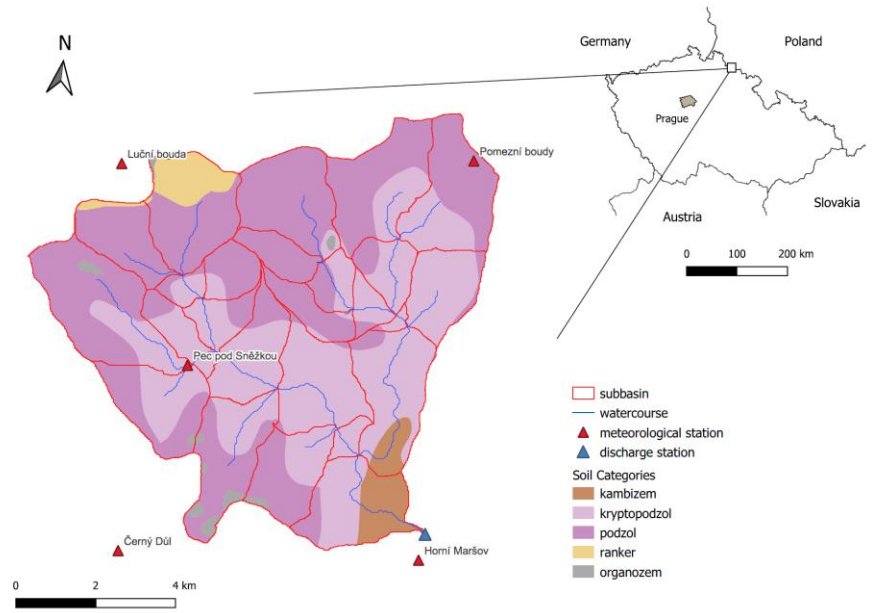

Fig. 1 Overview of the soil types distribution at the Horní Úpa catchment.

Tab. 1 Data sources for land cover analysis. The years where it was possible to produce annual cloud-free mosaics of satellite data are indicated by crosses on green shading. Orange shading marks the periods when a two- or three-year composite was used (from the DOY 150–270 imagery only). Percentile L5/L8 is equal to the threshold used for creating the cloud-free composite. The availability of aerial imagery used for training data collection is indicated by crosses in the AO column.

Year	Landsat sensor		AO	Year	Landsat sensor	Percentil	AO

	L5/TM	L7/ETM+	L8/OLI	Percentil L5/L8	
1991	x			40	
1992	x			50	
1993					
1994	x			40	
1995	x			40	
1996					
1997	x			40	x
1998					
1999	x	x		60	
2000	x	x		40	x
2001	x	x		40	x
2002	x	x		60	
2003	x			40	
2004	x			40	x
2005	x			40	x
2006	x	x		50	

	L5/TM	L7/ETM+	L8/OLI	L5/L8	
2007	x			40	x
2008					
2009	x			40	
2010	x			40	x
2011	x			40	x
2012					
2013			x	50	
2014					x
2015					
2016			x	50	x
2017					
2018			x	50	x
2019			x	50	
2020			x	50	x
2021					
2022			x	50	x

Tab. 2 Classified land cover classes for the SWAT hydrological model

Land cover class	SWAT code
Artificial surfaces (urban, road network)	URBN
Meadows and pastures	PAST
Broad-leaved forest	FRSD
Coniferous forest	FRSE
Dead coniferous forest	BSVG
Mixed forest	FRST
Transitional woodlands and shrubs	SHRB
Forest clearings and sparsely vegetated areas	BSVG
Dwarf pine shrubs	SBRB
Peat bogs	MIGM
Rocks	BARR
Water bodies and water courses	WATR

The resulting cloud-free mosaic contained six spectral bands of a given sensor, covering the visible, near, and mid-infrared parts of the spectrum, and calculated spectral indices suitable for monitoring vegetation condition - normalized difference vegetation index, normalized difference infrared index, normalized burn ratio, greenness, brightness and wetness of the Tasselled Cap (TC) transform (Crist and Cicone 1984). For the TC calculation, images containing the reflectance at the top of the atmosphere and the coefficients from Crist and Cicone (1984) for Landsat 5 and Baig et al. (2014) for Landsat 8 were used. Elevations from the SRTM model were added as an additional layer. Processing was automated using the

Google Earth Engine and the provided online access to the Landsat Collection 2 data (pre-processed by the US Geological Survey Earth Resources Observation and Science Center). The landcover classes correspond to the catchment conditions and to the requirements of the SWAT hydrological model. Overall, we used 12 land cover classes (see Table 2). A supervised approach was chosen for classification (Zagajewski et al. 2021; Potůčková et al. 2021). The collection of training sets since 1997 was done by visual interpretation of available colour (RGB or CIR) orthophotos with a spatial resolution of 0.2 to 0.5 m in combination with Landsat data. The orthophotos provided by the Krkonoše National Park Administration and the Czech Office for Surveying, Mapping and Cadastre were available online as Web Map Services (KRNAP 2025; ČÚZK 2025). In addition, a normalised digital surface model (nDSM) derived from airborne laser scanning was provided by the Krkonoše National Park Administration for the years 2018 and 2022 (KRNAP 2025) and was used to discriminate the transitional woodlands and coniferous forest in training data. In 2022, a field survey was conducted to refine some categories (especially transitional woodlands). For the 1991, 1992, and 1994 imagery, training sets were collected by interpretation of Landsat imagery only. The buildings and roads class were generated from OpenStreetMap (as downloaded on January 28, 2023) and used for all time horizons. The area is located in the highly protected zone of the national park and new constructions are therefore minimal. Similarly, the water class, which consists of only a few pixels in the 30 m resolution Landsat data, was vectorized over the orthophoto and included in the final classification.

The Random Trees algorithm, as implemented in ArcGIS Desktop v10 (Breiman 2001), was used for the classification. It is a non-parametric, robust classifier that can be applied to data of different scales. It provides information about the importance of each predictor. Moreover, the amount of training data required is smaller than for convolutional neural networks. Reflectivity values in six spectral bands, spectral indices, and height were used as features for classification, as mentioned above. Based on the tests performed, the classifier parameters were set to 300 trees and a maximum tree depth of 60.

To suppress random noise caused by the input data (radiometric values, training data), the following post-classification processing was carried out. First, we applied a majority filter to each single classification to remove pixels with a different class within or at the edge of homogeneous regions. Then, we defined a minimum classification mapping unit (1x 2 pixels), and finally smoothed the time series (i.e., removed unrealistic changes in land cover within the time series).

After post-processing, the resulting 12 land cover layers were the basis for further analyses. Classification accuracy was assessed based on stratified random sampling of 1500 points at the 95% two-sided confidence level (Foody, 2009). Classification classes were assigned to

validation points based on orthophoto interpretation; 94 of these points were validated in the field in 2022. Due to the time cost associated with the number of validation points and lack of aerial orthoimages in the 1990s, validation was only performed in 5 time-horizons (2001, 2010, 2016, 2018, 2022). A standard error of the area determined for each class could be estimated, based on Olofsson et al. (2014).

2.3 The SWAT hydrological model

2.3.1 The SWAT model fundamentals

The SWAT model used in the study is a comprehensive basin-scale, continuous-time model (Arnold et al. 2012). As a semi-distributed model, SWAT provides a high level of spatial discretization by dividing the original catchment into multiple subbasins. Subbasins are further subdivided into series of hydrological response units – i. e. hydrotope (HRUs), which represent unique combinations of slope, land use, and soil type.

The main components of the model are the modules of direct runoff (SURQ), evapotranspiration, soil water infiltration, subsurface lateral runoff (LATQ), groundwater runoff (shallow and deep aquifer) (GWQ), water reservoirs, nutrients, bacteria and others. Most of the above components are calculated separately for each HRU in a daily step. In the evapotranspiration section, the water retained by interception is estimated first for a given land cover category. The Priestley-Taylor method (Priestley and Taylor 1972) was chosen for the estimation of potential evapotranspiration. Actual evapotranspiration is then determined separately for soil and plants using the approach of Ritchie (1972).

2.3.2 Required input data

SWAT requires the following spatially distributed inputs for model building: a digital elevation model (DEM), soil type, and land use layers. The DEM from the Shuttle Radar Topography Mission (SRTM) at a spatial resolution of 30x30 m was used. The soil type map was obtained from the Soil Subtypes Map of the Czech part of the Elbe Basin, created by Němečková (2008).

The SWAT model requires daily climate data, including minimum and maximum air temperatures (TMP), precipitation (PCP), average wind speed (WIN), solar radiation (SOL) and relative humidity (HUM). Meteorological observations covering the period from 1990 to 2019 were obtained from five meteorological stations (Fig. 1) from the Czech Hydrometeorological Institute. SWAT assigns meteorological data from the closest station to the central point of the subbasin. Each subbasin was then divided into several elevation bands spanning for 100 m. For each elevation band, the correction for the average observed elevation gradient was applied both for air temperatures and precipitations.

2.3.3 Modelling procedure

The SWAT model was calibrated at the beginning of the period of available data using the corresponding land cover. Calibration and validation were conducted using the SWAT-CUP 2012 software (Abbaspour 2013) in combination with the Sequential Uncertainty Fitting 2 (SUFI-2) optimization algorithm. Performance evaluation of the best-fit simulations included objective functions such as percent bias (PBIAS) and Nash-Sutcliffe efficiency (NSE). For further information on these objective functions, refer to Moriasi et al. (2007).

Further several distinct land cover maps were designed for the assessment of land cover influence on catchment rainfall-runoff relationship and water balance. The specific land cover maps corresponded to documented differences in aerial representation of particular land-covers. In order to eliminate the influence of different climatic conditions on the modelling results the model was run separately for every land-cover set-up using the entire period of meteorological data 1991–2021, so that the runoff characteristics can be assessed using exactly the same meteorological data and not only the ones present in the period of land-cover. Altogether four land cover set-ups were assessed (thoroughly described in section 3.2) representing four land cover set-ups and both catchment water balance as well as the rainfall-runoff. The four land cover set-ups are denoted as LU1991, LU 2005, LU2011 and LU2022 always representing the land cover from particular year.

Finally, two extreme land cover scenarios were submitted to the hydrological model in order to check the sensitivity of the model results to pronounced changes in the land cover. In the first scenario, all areas originally attributed to transitional woodlands and shrubs and dwarf pine shrubs categories were altered to coniferous forest representing the gradual afforestation of the area induced by climate change. And in the second scenario, all coniferous forests were turned into transitional woodlands and shrubs, which may occur due to a bark beetle outbreak in the area.

3. Results

3.1 Calibration of the SWAT model

The hydrological model SWAT was calibrated in the period of 1993–1997. This period contains both wet (1995, 1997), dry (1996) and average years (1993, 1994) as recommended by Moriasi et al. (2007). The first two years of the available data were used as model warm-up. A total of 15 parameters were selected for the one-at-time sensitivity analysis. The selection of the parameters was based on a literature review on the application of SWAT models in streamflow and soil water calibration (Abbaspour 2015).

Within the calibration period, Nash-Suctliffe coefficient value of 0.47 was achieved for Horní Úpa watershed. In the validation period, the coefficient value was 0.50. The values of the Nash-Sutcliffe coefficient are satisfactory according to Moriasi et al. (2007), although there

are at the lower acceptable margin. Largest discrepancies between modelled and observed discharges were found for winter and spring periods due to the uncertain estimation of snow accumulation and snow melt in particular dormant seasons. The Nash-Sutcliffe coefficient ranged from 0.22 in the worst-performing year (2012) to 0.76 in the best-performing simulation year (2007). The catchment water balance is correctly simulated as simulated runoff equaled to 98.9% of the observed one in the entire period of 31 simulated years. Only 20% (calibration) and 18% (validation) of the measured data were not enclosed by the 95PPU band.

3.2 Land cover characteristics

3.2.1 Classification accuracy

The assessment of land cover change was preceded by an analysis of the classification accuracy achieved in five time-horizons according to the methodology procedure outlined at the end of Section 2.2. The hydrological analysis focused on seven vegetation categories (i.e., grassland, coniferous, mixed, and broad-leaved forest, transitional woodlands, dwarf pine shrubs, clearings and areas with sparse vegetation) and rocks. As the classes of built-up and water areas were not of interest and were masked for the classifications, they were not included in the accuracy assessment. Table 3 shows that the overall classification accuracy was between 70 and 80%. Mixed and broad-leaved forest proved to be the most problematic categories, with both confusion between these two categories and confusion between mixed and coniferous forest and transitional woodlands. For each validation dataset, the area standard error was estimated for each class (Olofsson et al. 2014). The median of standard error calculated from the five validation observations was used as the best estimate of the achievable accuracy of area determination for a given category. Based on this, the significance of the difference in area of a given category between two consecutive time horizons was assessed using a 95% confidence interval. Significant changes are highlighted in Table 4. In general, the number of significant changes was low, with the most pronounced ones observed between 1992 and 1994 and between 2002 and 2003.

Tab. 3 Classification accuracy expressed in terms of F1-score and overall accuracy (OA) is based on 1,500 validation points obtained by visual interpretation of RGB and CIR aerial orthophotos with a spatial resolution of 0.2 m to 0.5 m

	Landsat 8			Landsat 5	
	2022	2018	2016	2010	2001
	F1-score				
Meadows, pastures	0.91	0.83	0.89	0.86	0.75
Broad-leaved forest	0.53	0.56	0.73	0.60	0.56
Coniferous forest	0.89	0.88	0.89	0.80	0.92

Dead coniferous forest	0.75	0.56	0.71	-	-
Mixed forest	0.57	0.53	0.61	0.42	0.43
Transitional woodlands, shrubs	0.77	0.75	0.76	0.64	0.65
Clearings, sparsely vegetated areas	0.78	0.55	0.71	0.39	0.42
Dwarf pine shrubs	0.91	0.80	0.82	0.82	0.72
Peat bogs	0.98	0.93	0.85	0.68	0.83
Rocks	0.84	0.82	0.79	0.91	0.77
Overall Accuracy					
OA	**0.82**	**0.78**	**0.81**	**0.70**	**0.70**

3.2.2 Land cover change

The result of the land cover classification from Landsat satellite data in the initial reference year 1991 and final year 2022 is shown in Figure 2. Based on the classification, the area of each land cover class was calculated for each time horizon, see Table 4. According to the average values for the whole study period, coniferous forests (39%), transitional woodlands (29%) and meadows (10%) represent the highest proportion of the total classified area. The categories with a representation of less than 1% are peat bogs, water, and dead coniferous forest.

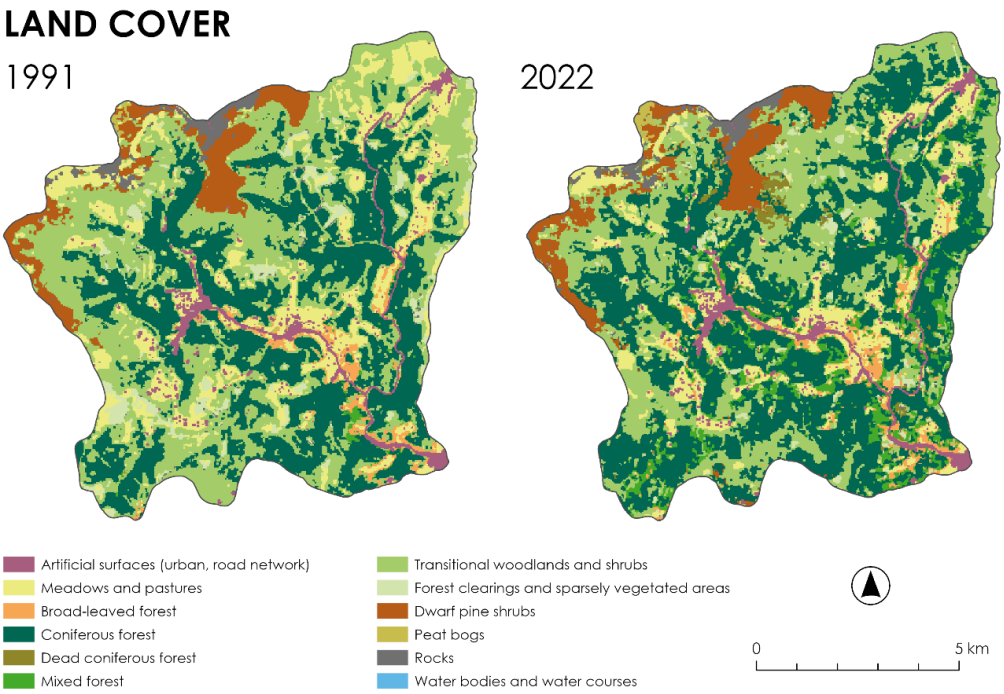

Fig. 2 Land cover classification from satellite images acquired by TM mapper and OLI sensors from Landsat 5 and Landsat 8 satellites, respectively, at the beginning and the end of the observed period (1991–2022).

Changes in land cover categories within the time series can be used to express the dynamics of the development dynamics of the studied area of interest. The spatial distribution of pixels with unchanged categories throughout the time series, i.e., stable areas, and conversely, the number of changes in each pixel, is shown in Figure 3. Stable areas represent 42.7% of the area of interest. The proportion of stable forest categories in the total area of the study catchment is as follows: deciduous forest 0.6%, mixed forest 0.2%, coniferous forest 20.4%, transitional woodlands 6.5%. Moreover, a detailed study of changes revealed that on 6.5% of the area, the change between matured deciduous, coniferous, and mixed forest categories occurred twice or more times. Similarly, pixels with repeated occurrences of dwarf pine shrubs, which do not belong to categories with high dynamics, represent 6.8% of the area. Such 'changes' indicate higher uncertainty in class distinction between the categories and may be attributed to classification inaccuracy rather than real change.

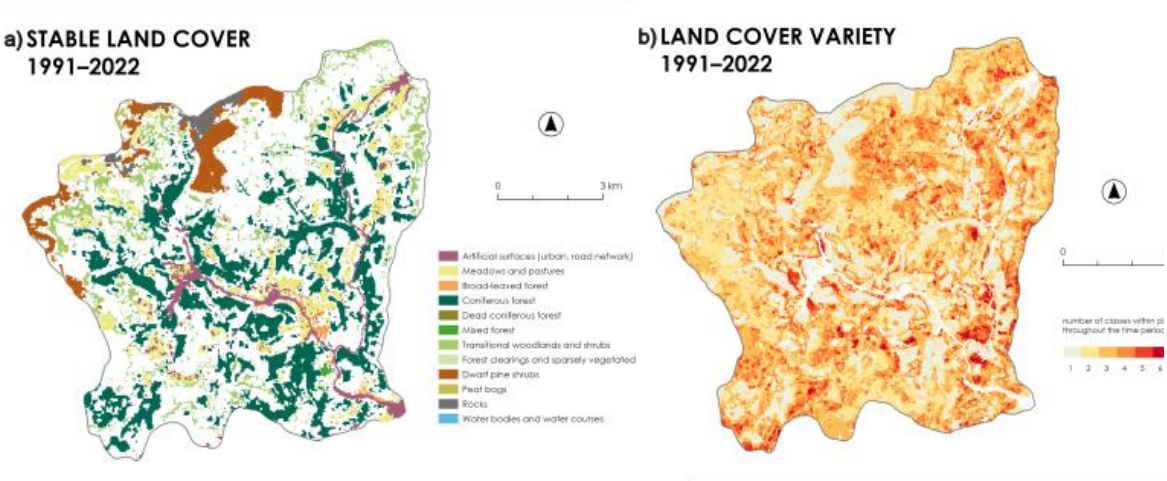

Fig. 3 Map of stable areas in Horní Úpa based on the classification of the satellite image time series between 1991 and 2022 (a). Pixels whose class has not changed over the entire time series are marked as stable. The number of land cover changes (variety) in a given pixel reflecting the dynamics of the area (b).

Breakpoints in the time series of the calculated areas of each category were sought. Figure 4 depicts an example of the two most represented categories, coniferous trees and transitional woodlands. For coniferous trees and transitional woodlands, the most significant breaks in the time series occurred in 1995, 2001, and around 2005. The period between 1991 and 2005 is characterised by forest maturation, when the area of coniferous forest increased from its minimum (30 km^2) to its maximum (39 km^2), while the area of transitional forest decreased from its maximum (34 km^2) to its minimum (23 km^2). These trends changed after 2005. Since 2011 there has been no significant change. Both categories tend to decrease slightly. Based

on this analysis four land covers maps were designed representing the land cover form the year 1991, 2005, 2011 and 2022 (denoted as LU1991, LU2005, LU2011 and LU2022).

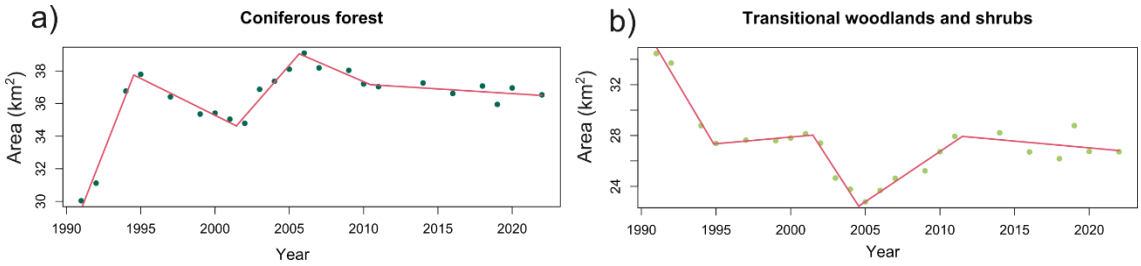

Fig. 4 Result of piecewise regression (red line) on the time series of the area calculated from Landsat image classification for the categories coniferous forest (a) and transitional woodlands (b). The main breakpoints are represented by the years 1995, 2001, and 2005 (or 2006 for the coniferous forest).

Tab. 4 Area of sub-categories based on land cover classification from Landsat data. The green and red colors highlight the maximum and minimum values for a given category. Orange shading indicates years with a change in the area of a given category above the 95% confidence interval (based on the median of standard errors shown in Appendix A1). For abbreviations of the land cover classes see Table 2

	Area [km^2]																								
	1991	**1992**	**1994**	**1995**	**1997**	**1999**	**2000**	**2001**	**2002**	**2003**	**2004**	**2005**	**2006**	**2007**	**2009**	**2010**	**2011**	**2014**	**2016**	**2018**	**2019**	**2020**	**2022**	Median	STD
URBN	4.23	4.23	4.23	4.23	4.23	4.23	4.23	4.23	4.23	4.23	4.23	4.23	4.23	4.23	4.23	4.23	4.23	4.23	4.23	4.23	4.23	4.23	4.23	4.23	0.00
PAST	12.71	**12.90**	10.77	10.75	11.09	11.95	11.26	10.86	10.93	8.84	8.58	8.35	8.43	9.06	9.24	8.10	7.84	8.42	8.36	7.71	**7.52**	7.86	8.25	8.84	1.69
FRSD	1.84	1.73	1.44	**1.44**	1.63	1.70	1.48	1.54	1.76	2.54	**2.86**	2.76	2.05	2.08	2.16	2.12	2.27	1.80	2.03	2.42	1.95	2.41	2.22	2.03	0.41
FRSE	**30.04**	31.12	36.77	37.79	36.41	35.36	35.41	35.04	34.79	36.87	37.36	38.11	**39.09**	38.19	38.03	37.20	37.03	37.26	36.62	37.08	35.95	36.96	36.53	36.87	2.10
BSVG																		**0.24**	0.63	0.50	0.77	0.80	**1.10**	0.70	0.29
FRST	**0.37**	0.46	2.19	2.31	2.34	2.87	3.39	3.81	4.26	7.53	8.06	**8.66**	6.56	6.02	5.29	4.76	4.43	5.97	6.82	5.41	4.47	5.23	5.96	4.76	2.23
SHRB	**34.45**	33.71	28.77	27.38	27.64	27.60	27.80	28.14	27.41	24.65	23.77	**22.77**	23.68	24.63	25.22	26.72	27.93	28.22	26.70	26.18	28.78	26.74	26.72	27.38	2.75
BSVG	3.38	2.89	2.03	2.39	3.03	2.51	2.28	2.41	2.44	2.88	2.69	2.50	2.19	2.21	2.37	**3.58**	2.95	**0.35**	1.10	2.73	2.64	1.99	1.68	2.44	0.69
SBRB	4.97	5.11	5.90	5.76	5.61	5.77	6.16	5.96	6.09	4.67	4.71	4.86	5.94	5.84	5.72	5.53	5.36	5.81	5.78	5.87	5.79	5.92	5.42	5.77	0.44
MIGM	**0.13**	0.14	0.15	0.18	0.22	0.23	0.22	0.22	0.24	0.17	0.18	0.18	0.23	0.23	0.24	0.20	0.22	0.24	0.25	**0.27**	0.26	0.24	0.26	0.22	0.04
BARR	**1.58**	1.41	1.45	1.47	1.50	1.49	1.46	1.48	1.56	1.31	1.26	1.28	1.30	1.20	1.20	1.24	1.43	**1.16**	1.18	1.30	1.33	1.31	1.32	1.32	0.13
WATR	0.00	0.00	0.00	0.00	0.00	0.00	0.00	0.00	0.00	0.00	0.00	0.00	0.00	0.00	0.00	0.00	0.00	0.00	0.00	0.00	0.00	0.00	0.00	0.00	0.0

3.3. Influence of land cover change on water budget and runoff

The following part is split into the assessment of evaluation of the gradual change of land cover on the hydrological regime of the Horní Úpa catchment and the water balance in hydrotopes covered with specific land cover.

3.3.1. Influence of land cover change on catchment runoff

The prominent source of information about land cover change influence on the catchment runoff characteristics are measured values of runoff in combination with precipitation sums. Hence first, the relationship between measured discharge and precipitation sums was analyzed by means of the double mass curve (Fig 5a). The curve demonstrates the stationary relationship between two observed variables from 1990 to 2014. After this breakpoint, less runoff was observed in comparison with precipitation sums. However, this was most probably caused by the occurrence of severe precipitation deficit during the drought period of 2014–2019 than by the changes in land cover. As mentioned in section 3.2, the most pronounced changes in land cover occurred from 1991 to 2005 and from 2005 to 2011. Since 2011 the spatial extent of particular land cover categories remained stable.

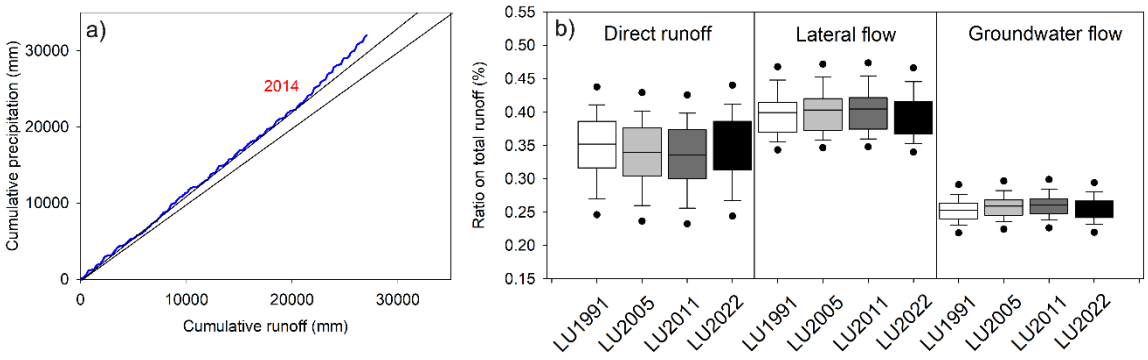

Fig. 5 Double mass curve and the ratio of direct (a), lateral subsurface and groundwater runoff in the period of 1991–2021 for all four land covers (b).

The documented change of land cover had only minor effect also on the modelled discharges as the long-term modelled average discharge differed only up to 3% among particular land cover set-ups. The only visible difference was that with increasing area covered with forest, more lateral subsurface and groundwater flow was produced at the expense of surface runoff. This was the case of set up representing the land cover from 2005 and 2011. However, the differences were up to 1.2% of the total runoff volume, hence statistically not significant (Fig. 5b). Nevertheless, the smaller extent of forest led to higher peak runoffs in a number of events (>25 $m^3.s^{-1}$).

3.3.2. Land cover influence on water balance

Most pronounced differences among investigated land covers were in terms of water partition in the soil profile into direct runoff, subsurface lateral flow and groundwater recharge with subsequent formation of groundwater contribution to streamflow. The differences in the rate of evapotranspiration were not statistically significant and merely not observable. This is given by the fact that under current climate conditions the mountainous regions are still energy limited in terms of evapotranspiration demand (Zelíková et al. 2025).

The fast direct runoff (SURQ) was highest (>600 mm.y^{-1}) in hydrotopes not covered by vegetation (BARR). Compared to all other land covers, it formed on average 2-3x more runoff. The lowest values of SRUQ were modelled from the forested areas (220-300 mm.y^{-1}). The average differences among forest types were at maximum 80 mm.year^{-1}. Among all three forest types, the highest SURQ was observed in deciduous forests and the lowest in mixed forests. All other land covers comprising pastures (PAST) and land with shrubs (SHRB) or sparse vegetation (BSVG) attained higher long-term averages of SURQ of 413, 326 and 349 mm.year^{-1}, respectively. The differences were more pronounced both in above-average wet and above-average dry years with dry years being most variable. SURQ was observed significantly more in winter months, only in the case of BARR there is no difference between summer and winter season (Fig. 6).

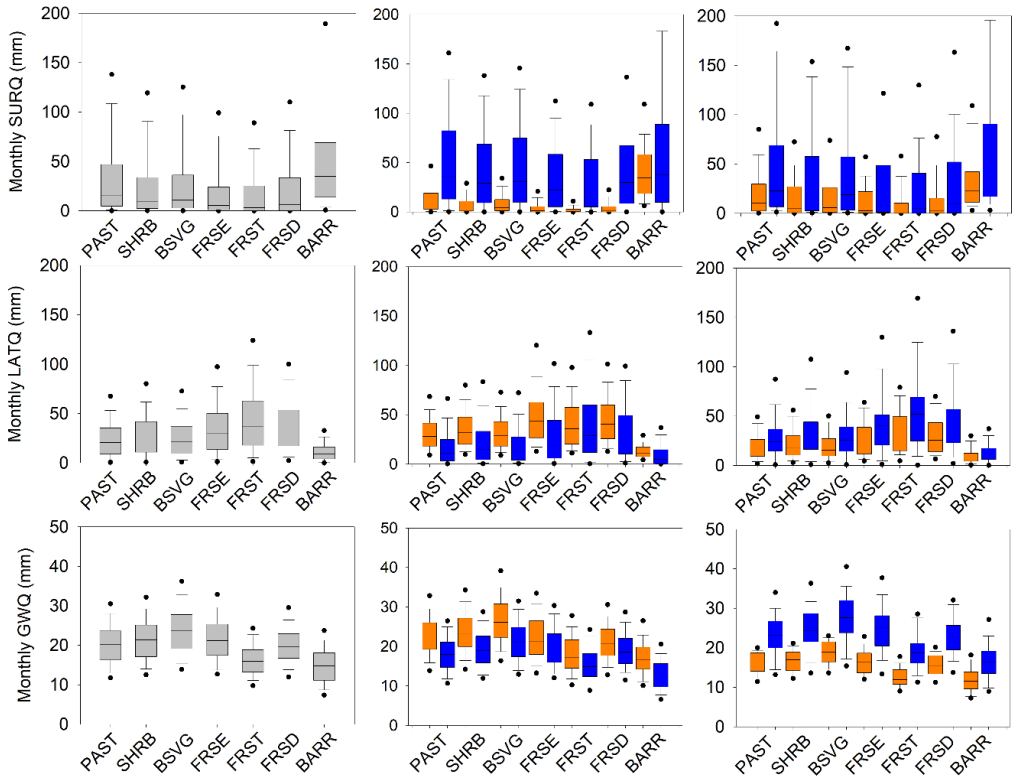

Fig. 6 Monthly sums of investigated water fluxes (SURQ, LATQ, GWQ in rows) in 1991–2021 for all hydrotopes divided according land cover categories (shortcuts explained in Table 2). The first column: annual sums, the second column: sums for summer (orange) and winter

(blue), the third column: a 3-year period of wet (blue) (2000–2002) and dry (orange) (2014–2016) years.

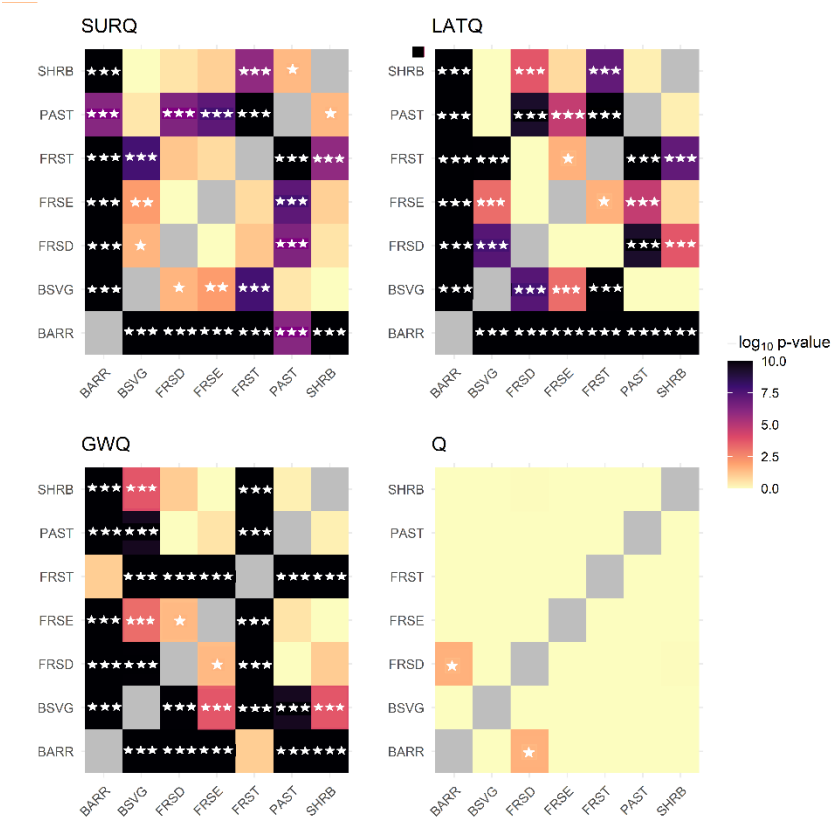

Fig. 7 Results of the Kruskal-Wallis test across all landcovers and inspected seasons. Crosses indicate significantly different means (at the 5%, 2,5% and 1% significance level) and colours indicate the strength of a relationship.

On the other hand, the lateral subsurface flow (LATQ) was formed at highest rate in forested hydrotopes forming average annual values of runoff from 450 to 550 mm.y^{-1}. The highest LATQ was on average formed in mixed forest (554 mm.year^{-1}), followed by deciduous forest (477 mm.year^{-1}) and finally the less prone was evergreen forest (438 mm.year^{-1}). Apart from forested hydrotopes, LATQ formation ranged between 300 and 400 mm.y^{-1} in pasture, shrubland and sparse vegetation covered hydrotopes. LATQ from pasture and shrubland covered hydrotopes statistically differ from the rest. Areas covered by sole bare land attained significantly less LATQ (<150 mm.y^{-1}) as the soil profile is the shallowest. There are no profound changes in the described pattern in wet and dry periods (Fig. 6), only the values of LATQ are higher or lower. In summer season, the differences among hydrotopes with particular landcover were not statistically significant. In winter, only the deciduous forest significantly differed from other forest types and less vegetated surfaces (Fig. 7).

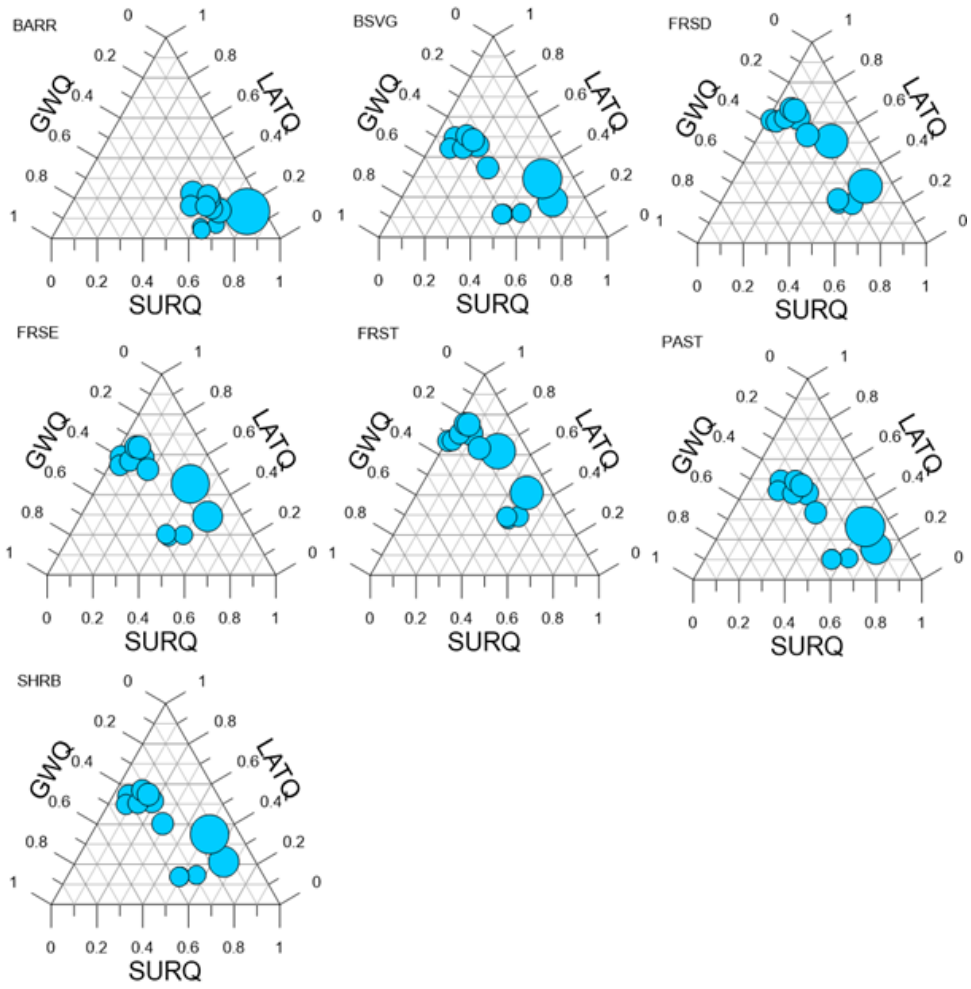

Fig. 8 Monthly average contributions to total runoff for hydrotopes covered by all seven inspected landcovers (indexes explained in Table 2). Obtained as an average from the SWAT model simulation in 1991–2021. GWQ, LATQ and SURQ represent groundwater, subsurface lateral and direct flow.

The average annual values of groundwater contribution to runoff (GWQ) ranged from 179 $mm.y^{-1}$ in the hydrotopes without vegetation cover to 289 $mm.y^{-1}$ in the hydrotopes with sparse vegetation. Vegetated hydrotopes (PAST, SHRUB, FRSD, FRSE) attained average annual rates of groundwater flow from 241 to 260 $mm.y^{-1}$. Lower rate of groundwater flow was modelled for the mixed forest hydrotopes (197 $mm.y^{-1}$) as lateral subsurface flow was estimated to be the major flow pathway. All forested sites differed significantly from each other. Similarly, as for the LATQ, the same pattern of GWQ rates was observed among hydrotopes with particular land cover for summer periods and little less differences in winter period. The same applies for the dry and wet years, respectively.

The long-term average contributions of all three types of runoff for particular land covers are shown in Fig. 8. It demonstrates that in hydrotopes covered by bare soil, the direct runoff formed 63% of total runoff on average and this percentage was stable over the course of the year. Only 13% of runoff was modelled to be formed by lateral subsurface flow and less than

25% by the groundwater contribution. In the hydrotopes covered by sparse vegetation, the average contribution of all runoff types was merely equal (33% SURQ, 33% LATQ, 34% GWQ) with surface runoff dominating in the winter and equal contribution of direct and lateral flow in summer (~45%). The prevailing winter role of surface runoff was observed in all inspected hydrotopes documented by a distinct group of circles (December to April) in the right-hand side of the triangle plots (Fig. 8). This is given by the saturated soil in this period resulting in propensity of melt/rainwater to flow over soil surface or through the soil profile using shallow lateral pathways. In areas covered by shrubs and pastures, the lateral flow dominated summer runoff (~45%) with groundwater flow forming 30–40%. Lateral flow was on average highest in forest-covered hydrotopes (>45%), especially in mixed forests where it attained 56.5% of total runoff on average. The groundwater contribution in the forested sites ranged from 22.2% (FRST), over 25.8% (FRSD) to 30.5% (FRSE). Direct flow was least prominent in the forest-covered sites contributing up to 10% of runoff in summer. In summer months, mixed forests differed from evergreen and deciduous ones by higher contribution of lateral subsurface flow (groundwater flow at the expense of direct (up to 5%) and groundwater flow contributions.

3.3.3 Influence of two extreme land cover scenarios on catchment water balance

Deforestation represented by the change of all areas covered by conifer forest to transitional woodlands and shrubs led to slightly higher peak discharges and faster recession to baseflow. On average, twenty peak discharges were higher by 6.6%. The total runoff volume increased only by 2.7% compared to the reference scenario which was represented by the land cover from 1991. The surface runoff contribution to total runoff increased by 4.1% on average (1991-2021) at the expense of lateral subsurface runoff and groundwater runoff contributions, which decreased by 4.0% and 0.6%, respectively. Contrarily afforestation of the transitional areas led to slightly lower peak discharges and non-detectable changes in the recession limb of the hydrographs. The average decrease of the twenty peak discharges was 0.8%. Surface runoff decreased by 1.8% on average and it was compensated by the increase of groundwater contribution to runoff. The total runoff volume increased by 2.7% when the area was deforested and decreased by 0.8% when it was afforested. The overall influence of forest thinning and contrarily afforestation of all transitional woodlands and shrubs led only to minor changes in runoff volumes, timing and other runoff characteristics.

4. Discussion

4.1 Land cover classification

The Landsat data classification showed that at least 42.7% of the area of interest remained stable between 1991 and 2022. Although the overall accuracy for selected time horizons was only 70–80%, it is comparable to other studies that used Landsat data to quantify changes in different temperate forest types (Griffiths et al. 2014; Zagajewski et al. 2021) or forest disturbances (Senf et al. 2017) over decades. However, so far the Landsat archive is the only one that can provide consistent multispectral data continuously for such a long period. Analysis of the time series of areas derived from the classification of each category revealed significant breakpoints in 1995, 2001, 2005, and 2011. Communication with experts from the KRNAP National Park Administration confirmed the observed changes in coniferous forest. Its increase from 1991, the beginning of the observation period, to 1995 can be attributed to the growth of forest plantations following extensive damage to Norway spruce stands in connection with huge immission loads in the 1980s (Vacek et al. 1999). The slight decline from 1997 onwards was due to damages caused by icing. After a period of recovery between 2001 and 2006, the cyclonic storm Kyrill in 2007 followed by repeated bark beetle outbreaks, are the main factors for the subsequent decline of coniferous forest in the studied catchment (ÚHÚL 2022).

In central European mountainous environments such as the Krkonoše Mts., the Krušné Mountains or the Tatra Mountains, land cover changes have been extensively studied, particularly in relation to the decline of spruce-dominated forests due to air pollution, bark beetle outbreaks and wind disturbances (Zagajewski et al. 2021, Kupková et al. 2018). The expansion of subalpine shrubland and secondary succession in formerly forested areas has been documented through remote sensing analysis, highlighting the influence of climate change and disturbance regimes on vegetation dynamics (Arekhi et al. 2018, Mašek et al. 2023). Additionally, historical aerial imagery has been used to reconstruct long-term land cover trajectories, revealing for example shrub encroachment due to artificial planting of the dwarf pine in the past as well as the cessation of former farming and, most probably, also by global change in the KRNAP National Park (Potůčková et al. 2021).

4.2 Input data and hydrological modelling

The input data and the performance of the hydrological model are subject to various uncertainties. One major source of bias is the underestimation of precipitation when using standard rain gauges. This occurs because rain gauge measurements often contain significant errors, particularly during the winter months (Dingman 2015). Even after corrections, the accuracy of winter precipitation estimates remains uncertain (error up to 40% precipitation volume), as measuring precipitation in mountainous regions involves several challenges and limitations (Sevruk 2005).

The hydrological SWAT was chosen as a modelling tool as it is commonly used for the assessment of land cover change influence on the hydrological regime (Siqueira et al. 2021; Valencia et al. 2024). The primary limitation in the model's performance stemmed from the snowmelt and snow accumulation/melt routine, which relied on the degree-day approach. However, it was documented that the degree-day approach proved to be the second-best choice (radiation balance approach was not chosen as the data were not available) for the modelling of snowmelt dynamics in Central Europe (Girons Lopez et al., 2020). The representation of particular processes representing the evaporation from the catchment also contains several crucial simplifications that do not take into account the non-stationary character of rainfall interception in the mountainous regions (Kofroňová et al., 2021), the differences in physiological response of different vegetation to drought-stress (Gebhardt et al. 2023) or forest floor evaporation (Floriancic et al. 2023). All these model simplifications can cause less pronounced effect of land cover change on hydrological régime of the area (Fatichi et al. 2016). Hence, the results of such studies represent the lower boundary of future possible development.

4.3 The influence of land cover change on the hydrological regime

The observed changes of land cover in Upper Úpa catchment did not cause any significant alternation of the hydrological regime. However, we have observed significant changes in runoff generation among inspected landcovers, namely in the representation of direct runoff and deeper and slower pathways represented by subsurface lateral and groundwater flows. It is necessary to stress that the observed changes in runoff generation processes are results of the modelling exercise and it was not observed in the real environment. A brief investigation of precipitation patterns preceding the modelling itself revealed no shift in daily precipitation totals in the ten-year periods of 1990–2000, 2001-2010, and 2011-2021, and thus climate-induced changes should not represent a significant contributing factor to the presented results. In Central Europe, the non-detectable changes in hydrological regime despite changes in land cover were also reported by Bernsteinová et al. (2015) in Šumava Mts. and Wojkowski et al. (2022) in Upper Vistula basin. All these changes were only of local importance and they were probably dampened on the larger scale of gauging station, which was hypothesized by Blöschl et al. (2007). It needs to be stressed that these studies are limited to mountainous areas having high precipitation sums and low evapotranspiration. This possibly stands behind negligible differences in actual evapotranspiration among particular vegetation covers. We hypothesize that the differences in actual evapotranspiration will be larger in lower altitudes with more favorable meteorological conditions (Ji et al. 2024), lower amount of deposited

water (influencing the importance of interception) and occurrence of soil water deficits will play more important role.

Experiments aimed at revealing the influence of extreme land cover changes on the local hydrology showed that changes from all coniferous forest to transitional woodlands and shrubs (including dwarf pine) and vice versa did not cause significant changes in the results of the hydrological modelling. The modelled changes affected about 30% of the catchment area. Thus, the real changes in the area of land cover classes, which reach a maximum of 12% of the study area (corresponding to the change of transitional woodlands between 1991 and 2005), as well as the accuracy gained, do not have a major impact on the changes in runoff.

5. Conclusion

This study aimed to quantify land cover change in a mid-latitude mountainous catchment over the past 30 years, to represent the catchment water balance using a semi-distributed hydrological model, and to assess the influence of time-varying land cover on the hydrological response, including afforestation and deforestation scenarios.

The land cover analysis captured the main patterns of vegetation change, including the transition from coniferous forests to transitional woodland-shrub and the gradual increase in mixed forests at the expense of grasslands. The influence of disturbance events, such as windthrows and bark beetle outbreaks, was evident, especially after 2007. Although finer-scale structural changes in vegetation could not be fully resolved, the results offered a sufficiently robust basis to explore long-term shifts in vegetation cover and their potential hydrological implications.

The hydrological simulations indicated that land cover changes had only a limited impact on the overall water balance, while influencing the partitioning between different runoff components. The results suggest that the Horní Úpa catchment exhibits a certain resilience to land cover variability under current climatic conditions. However, these results are not generally applicable, they apply only on the impact of land cover change of mountainous forest-dominated catchments. Additionally, the static representation of land cover and soils in the SWAT model, together with the fixed delineation of hydrological response units, may have constrained the model's sensitivity to more subtle changes in vegetation dynamics.

Despite these limitations, the study provides an important contribution to the understanding of interactions between land cover change and hydrological processes in complex mountainous environments. It demonstrates the potential of combining satellite-based land cover mapping with process-based hydrological modelling to explore landscape-hydrology linkages over long timescales. Future research should focus on integrating higher-resolution and temporally dynamic land cover data, improving field-based validation, refining soil and

vegetation parameterization, and employing models capable of capturing dynamic vegetation processes. Additionally, we encourage analogous studies in catchments with different topography, climate, soil and land cover characteristics. These steps will help to further enhance the reliability of hydrological assessments under changing land use and climate conditions in sensitive mountain catchments such as the Krkonoše Mountains.

Acknowledgments

This work was supported by the Technological Agency of the Czech Republic (SS05010124), the institutional support of the Czech Academy of Sciences (RVO: 67985874).

References

Abbaspour, K. C. (2013): SWAT-CUP 2012: SWAT calibration and uncertainty programs – A User manual. Swiss Federal Institute of Aquatic Science and Technology, Eawag

Abbaspour, K. C., Rouholahnejad, E., Vaghefi, S., Srinivasan, R., Yang, H., Kløve, B. (2015): A continental-scale hydrology and water quality model for Europe: Calibration and uncertainty of a high-resolution large-scale SWAT model. J Hydrol (524), 733–752. https://doi.org/10.1016/j.jhydrol.2015.03.027

Alaoui, A., Lipiec, J., Gerke, H. H. (2011): A review of the changes in the soil pore system due to soil peformation: A hydrodynamic perspective. Soil Till Res (115–116), 1–15. https://doi.org/ 10.1016/j.still.2011.06.002

Archer, N. A. L., Bonell, M., Coles, N., MacDonald, A. M., Auton, C. A., Stevenson, R. (2013): Soil characteristics and landcover relationships on soil hydraulic conductivity at a hillslope scale: A view towards local flood management. J Hydrol (497), 208–222. https://doi.org/10.1016/j.jhydrol.2013.05.043

Arekhi, M., Yesil, A., Ozkan, U. Y. et al. (2018): Detecting treeline dynamics in response to climate warming using forest stand maps and Landsat data in a temperate forest. For Ecosyst (5), 23. https://doi.org/10.1186/s40663-018-0141-3

Arnold, J. G., Moriasi, D. N., Gassman, P. W., Abbaspour, K. C., White, M. J., Srinivasan, R., Santi, C., Harmel, R.D., Van Griensven, A., Van Liew, M.W., Kannan, N., Jha, M.K. (2012): SWAT: model use, calibration, and validation. Trans ASABE 55(4):1491–1508. http://dx.doi.org/10.13031/2013.42256

Baig, M.H.A., Zhang, L., Shuai, T., Tong, Q. (2014): Derivation of a tasselled cap transformation based on Landsat 8 at-satellite reflectance. Remote Sens Lett 5(5): 423–431. https://doi.org/10.1080/2150704X.2014.915434

Bebi, P., Seidl, R., Motta, R., Fuhr, M., Firm, D., Krumm, F., Conedera, M., Ginzler, C., Wohlgemuth, T., Kulakowski, D. (2017): Changes of forest cover and disturbance regimes in the mountain forests of the Alps. For Ecol Manag (388), 43–56. https://doi.org/10.1016/j.foreco.2016.10.028

Bernsteinová, J., Bässler, C., Zimmermann, L., Langhammer, J., Beudert, B. (2015): Changes in runoff in two neighbouring catchments in the Bohemian Forest related to climate and land cover changes. J Hydrol Hydromech (63), 342–352. https://doi.org/: 10.1515/johh-2015-0037

Blackburn, D.A., Oliphant, A.J., Davis, J.D. (2021): Carbon and Water Exchanges in a Mountain Meadow Ecosystem, Sierra Nevada, California. Wetlands (41), 39. https://doi.org/10.1007/s13157-021-01437-2

Blöschl, G., Ardoin-Bardin, S., Bonell, M. et al. (2007): At what scales do climate variability and land cover change impact on flooding and low flows? Hydrol Process (21), 1241–1247. https://doi.org/10.1002/hyp.6669

Blöschl, G. (2022): Three hypotheses on changing river flood hazards. Hydrol Earth Syst Sci 26(19): 5015–5033. https://doi.org/10.5194/hess-26-5015-2022

Breiman, L. (2001): Random Forests. Mach Learn (45), 5–32. https://doi.org/10.1023/A:1010933404324

Chaves, M.E.D., Picoli, M.C.A., Sanches, I.D. (2020): Recent Applications of Landsat 8/OLI and Sentinel-2/MSI for Land Use and Land Cover Mapping: A Systematic Review. Remote Sen (12), 18, 3062. https://doi.org/10.3390/rs12183062

Chen, Z., Wang, W., Woods, R.A., Shao, Q. (2021): Hydrological effects of change in vegetation components across global catchments. J Hydrol (595), 125775. https://doi.org/10.1016/j.jhydrol.2020.125775

Cognard-Plancq, A.L., Marc, V., Didon-Lescot, J.F., Normand, M. (2001): The role of forest cover on streamflow down sub-Mediterranean mountain watersheds: a modelling approach. J Hydrol (254: 1-4), 229-243. https://doi.org/10.1016/S0022-1694(01)00494-2

Crist, E.P., Cicone, R.C. (1984): A physically-based transformation of Thematic Mapper data – The TM Tasseled Cap. IEEE Trans Geosci Remote Sens (3), 256–263. https://doi.org/10.1109/TGRS.1984.350619

ČÚZK - Český úřad zeměměřický a katastrální (Czech Office for Surveying, Mapping and Cadastre) (2025). Geoprohlížeč [Online]. Available at: https://ags.cuzk.gov.cz/geoprohlizec/ [11-10-2025].

Danáčová, M., Földes, G., Labat, M.M., Kohnová, S., Hlavčová, K. (2020): Estimating the effect of deforestation on runoff in small mountainous basins in Slovakia. Water (12), 11, 3113. https://doi.org/10.3390/w12113113

Dingman, S.L. (2015): Physical hydrology, 3. ed. Waveland Press, Inc., Long Grove. doi:10.1177/030913338901300106

Dubbert, M., Werner, C. (2018): Water fluxes mediated by vegetation: emerging isotopic insights at the soil and atmosphere interfaces. New Phytol (221: 4), 1754–1763. https://doi.org/10.1111/nph.15547

Fatichi, S., Vivoni, E.R., Ogden, F.L. et al. (2016): An overview of current applications, challenges, and future trends in distributed process-based models in hydrology. J Hydrol (537), 45–60. https://doi.org/10.1016/j.jhydrol.2016.03.026.

Feranec, J., Solin, L., Kopecká, M., Oťahel, J., Kupková, L., Štych, P., Bičík, I., Kolář, J., Čerba, O., Soukup, T., Brodský, L. (2014): Analysis and expert assessment of the semantic similarity between land cover classes. Progress in Physical Geography. 28/3, s. 301 – 327. https://doi.org/10.1177/0309133314532001

Feranec, J., Soukup, T., Hazeu, G., Jaffrain, G. (2016): European landscape dynamics: CORINE land cover data. CRC Press, London.

Floriancic, M.G., Allen, S.T., Meier, R., Truniger, L., Kirchner, J.W., Molnar, P. (2022): Potential for significant precipitation cycling by forest-floor litter and deadwood, Ecohydrology (16), 1–16. doi:10.1002/eco.2493

Foody, G.M. (2009): Sample size determination for image classification accuracy assessment and comparison. Int J Remote Sens (30), 5273–5291. https://doi.org/10.1080/01431160903130937

Gao, L., Wang, X., Johnson, B.A., Tian, Q., Wang, Y., Verrelst, J., Mu, X., Gu, X. (2020): Remote sensing algorithms for estimation of fractional vegetation cover using pure vegetation index values: A review. ISPRS J Photogramm (159), 364–377. https://doi.org/10.1016/j.isprsjprs.2019.11.018.

Gebhardt, T., Hesse, B.D., Hikino, K., Kolovrat, K., Hafner, B.D., Grams, T.E.E., Häberle, K.H. (2023): Repeated summer drought changes the radial xylem sap flow profile in mature Norway spruce but not in European beech. Agric For Meteorol (329), 109285. doi:10.1016/j.agrformet.2022.109285.

Girons Lopez, M., Vis, M.J.P., Jenicek, M., Griessinger, N., Seibert, J. (2020): Assessing the degree of detail of temperature-based snow routinesfor runoff modelling in mountainous areas in central Europe. Hydrol Earth Syst Sci (24), 4441–4461. https://doi.org/10.5194/hess-24-4441-2020

Green, W.H., Ampt, G.A. (1911): Studies on soil physics: 1. The flow of air and water through soils. J Agric Sci (11–24).

Griffiths, P., Kuemmerle, T., Baumann, M. et al. (2014): Forest Disturbances, Forest Recovery, and Changes in Forest Types across the Carpathian Ecoregion from 1985 to

2010 Based on Landsat Image Composites. Remote Sensi Environ (151), 72–88. https://doi.org/10.1016/j.rse.2013.04.022

Healey, S.P., Cohen, W.B., Zhiqiang, Y., Krankina, O.N. (2005): Comparison of tasseled cap-based Landsat data structures for use in forest disturbance detection. Remote Sens Environ (97: 3), 301-310. https://doi.org/10.1016/j.rse.2005.05.009

Huang, C., Goward, S.N., Masek, J.G., Thomas, N., Zhu, Z., Vogelmann, J.E. (2010): An automated approach for reconstructing recent forest disturbance history using dense Landsat time series stacks. Remote Sens Environ (114: 1), 183–198. https://doi.org/10.1016/j.rse.2009.08.017

Jasechko, S., Sharp, Z.D., Gibson, J.J., Birks, J., Yi, Y., Fawcett, P.J. (2013): Terrestrial water fluxes dominated by transpiration. Nature (496), 347–350. https://doi.org/10.1038/nature11983.

Jaworek-Jakubska, J., Filipiak, M., Napierała-Filipiak, A. (2020): Understanding of Forest Cover Dynamics in Traditional Landscapes: Mapping Trajectories of Changes in Mountain Territories (1824–2016), on the Example of Jeleniogórska Basin, Poland. Forests (11: 8), 867. https://doi.org/10.3390/f11080867

Ji, Z., Wang, Y., Wang, L. (2024): Threshold identification of evapotranspiration under different land-use types in the Loess Plateau, China. J Hydrol Reg (53), 101780. https://doi.org/10.1016/j.ejrh.2024.101780

Knisel, W.G. (1980): CREAMS: a field scale model for Chemicals, Runoff, and Erosion from Agricultural Management Systems [USA]. Environ Sci (26), 643–659.

Kofroňová, J., Šípek, V., Hnilica, J., Vlček, L., Tesař, M. (2021): Canopy interception estimates in a Norway spruce forest and their importance for the hydrological modelling. Hydrol Sci J (66: 7), 1233–1247. https://doi.org/10.1080/02626667.2021.1922691

KRNAP – Krkonošský národní park (Krkonoše National Park Administration) (2025). Veřejný mapový portál [Online]. Available at: https://ags.krnap.cz/mapy/prohlizecka/ [11-10-2025].

Kupková, L., Potůčková, M., Lhotáková, Z., Albrechtová, J. (2018): Forest cover and disturbance changes, and their driving forces: A case study in the Ore Mountains, Czechia, heavily affected by anthropogenic acidic pollution in the second half of the 20th century. Environ Res Lett (13: 9), 095008. https://doi.org/10.1088/1748-9326/aadd2c

Kupková, L., Bičík, I., Jeleček, L. (2021): At the Crossroads of European Landscape Changes: Major Processes of Landscape Change in Czechia since the Middle of the 19th Century and Their Driving Forces. Land 10. ISSN 2073-445X.

Kupková, L., Červená, L., Potůčková, M., Lysák, J., Roubalová, M., Hrázský, Z., Březina, S., Epstein, H.E., Müllerová, J. (2023): Towards reliable monitoring of grass species in nature

conservation: Evaluation of the potential of UAV and PlanetScope multi-temporal data in the Central European tundra. Remote Sens Environ (294), 113645. https://doi.org/10.1016/j.rse.2023.113645

Lachassagne, P., Wyns, R., Dewandel, B. (2011): The fracture permeability of Hard Rock Aquifers is due neither to tectonics, nor to unloading, but to weathering processes. Terra Nova (23: 3), 145–161. https://doi.org/10.1111/j.1365-3121.2011.00998.x

Launiainen, S., Guan, M., Salmivaara, A., Kieloaho, A.J. (2019): Modeling boreal forest evapotranspiration and water balance at stand and catchment scales: a spatial approach. Hydrol Earth Syst Sci (23: 8), 3457–3480. https://doi.org/10.5194/hess-23-3457-2019.

Mašek, J., Tumajer, J., Lange, J. et al. (2023): Shifting climatic responses of tree rings and NDVI along environmental gradients. Sci Total Environ (908), 168275. https://doi.org/10.1016/j.scitotenv.2023.168275

Meier, R., Schwaab, J., Seneviratne, S.I. et al. (2021): Empirical estimate of forestation-induced precipitation changes in Europe. Nat Geosci (14), 473–478. https://doi.org/10.1038/s41561-021-00773-6

Mensah, J.K., Ofosu, E.A., Yidana, S.M., Akpoti, K., Kabo-bah, A.T. (2022): Integrated modeling of hydrological processes and groundwater recharge based on land use land cover, and climate changes: A systematic review. Environ Adv (8), 100224. https://doi.org/10.1016/j.envadv.2022.100224

Moriasi, D.N., Gitau, M.W., Pai, N., Daggupati, P. (2015): Hydrologic and water quality models: performance measures and evaluation criteria. Trans ASABE (58: 6), 1763–1785. https://doi.org/ 10.13031/trans.58.1071

Němečková, S. (2008): The Map of soil subtypes of the Czech part of the Elbe river basin for the hydrological model SWIM. IH CAS, CD-ROM.

Nepstad, D.C., de Carvalho, C.R., Davidson, E.A. et al. (1994): The role of deep roots in the hydrological and carbon cycles of Amazonian forests and pastures. Nature (372, 6507), 666–669. https://doi.org/10.1038/372666a0

Olofsson, P., Foody, G.M., Herold, M., Stehman, S.V., Woodcock, C.E., Wulder, M.A. (2014): Good practices for estimating area and assessing accuracy of land change. Remote Sens Environ (148), 42–57. https://doi.org/10.1016/j.rse.2014.02.015

Pielke, R.A., Avissar, R., Raupach, M., Dolman, A.J., Zeng, X., Denning, A.S. (1998): Interactions between the atmosphere and terrestrial ecosystems: influence on weather and climate. Global Change Biol (4: 5), 461–475. https://doi.org/10.1046/j.1365-2486.1998.t01-1-00176.x

Potůčková, M., Kupková, L., Červená, L., Lysák, J., Krause, D., Hrázký, Z., Březina, S., Müllerová, J. (2021): Towards resolving conservation issues through historical aerial

imagery: vegetation cover changes in the Central European tundra. Biodivers Conserv (30), 3433–3455. https://doi.org/10.1007/s10531-021-02255-y.

Priestley, C.H.B., Taylor, R.J. (1972): On the assessment of surface heat flux and evaporation using large-scale parameters. Monthly Weather Review (100: 2), 81–92. https://doi.org/10.1175/1520-0493(1972)100<0081:OTAOSH>2.3.CO;2

Ramon, F.B., Millington, J.D.A., Moran, E.F., Batistella, M., Liu, J. (2020): Three decades of land-use and land-cover change in mountain regions of the Brazilian Atlantic Forest. Landsc Urban Plan (204), 103948. https://doi.org/10.1016/j.landurbplan.2020.103948.

Ritchie, J.T. (1972): A model for predicting evaporation from a row crop with incomplete cover. Water Resour Res (8), 1204–1213. https://doi.org/10.1029/WR008i005p01204

Senf, C., Pflugmacher, D., Hostert, P., Seidl, R. (2017): Using Landsat time series for characterizing forest disturbance dynamics in the coupled human and natural systems of Central Europe. ISPRS J Photogram and Remote Sens (130), 453–463. https://doi.org/10.1016/j.isprsjprs.2017.07.004.

Sevruk, B. (2005): Rainfall measurement: gauges. In: Anderson MG (ed) Encyclopedia of Hydrological Sciences, 3rd edn. Wiley, New York, pp. 230–257.

Sieker, F. (2000): Investigations of the effects of on-site stormwater management measures in urban and agricultural areas on floods. In: Marsalek et al (ed) Flood Issues in Contemporary Water Management. Springer Netherlands, Dordrecht, pp. 303–310.

Siqueira, P.P., Oliveira, P.T.S., Bressiani, D., Neto, A.A.M., Rodrigues, D.B.B. (2021): Effects of climate and land cover changes on water availability in a Brazilian Cerrado basin. J Hydrol Reg (37), 100931. https://doi.org/10.1016/j.ejrh.2021.100931

Sonnenborg, T.O., Christiansen, J.R., Pang, B., Bruge, A., Stisen, S., Gundersen, P. (2017): Analyzing the hydrological impact of afforestation and tree species in two catchments with contrasting soil properties using the spatially distributed model MIKE SHE SWET. Agricultural For Meteorol (239), 118–133. https://doi.org/10.1016/j.agrformet.2017.03.001

Sutanto, S.J., van den Hurk, B., Dirmeyer, P.A., Seneviratne, S.I., Röckmann, T., Trenberth, K.E., Blyth, E.M., Wenninger, J., Hoffmann, G. (2014): HESS Opinions "A perspective on isotope versus non-isotope approaches to determine the contribution of transpiration to total evaporation". Hydrol Earth Syst Sci (18), 2815–2827. https://doi.org/10.5194/hess-18-2815-2014

Talukdar, S., Singha, P., Mahato, S., Shahfahad, P.S., Liou, Y.A., Rahman, A. (2020): Land-Use Land-Cover Classification by Machine Learning Classifiers for Satellite Observations—A Review. Remote Sens (12: 7), 1135. https://doi.org/10.3390/rs12071135

Tolasz, R. (2007): Climate atlas of Czechia. Czech Hydrometeorological Institute, Prague

Trinh, D.H., Chui, T.F.M. (2013): Assessing the hydrologic restoration of an urbanized area via an integrated distributed hydrological model. Hydrol Earth SystSci (17: 12), 4789–4801. https://doi.org/10.5194/hess-17-4789-2013

ÚHÚL (2022): Oblastní plán rozvoje lesů: Přírodní lesní oblast 22 – Krkonoše. Analýza stavu a vývoje. ÚHÚL. Brandýs nad Labem – Stará Boleslav.

USDA SCS (1985): National Engineering Handbook, Section 4: Hydrology. Soil Conservation Service – USDA, Washington DC.

Vacek, S., Bastl, M., Lepš, J. (1999): Vegetation changes in forest of the Krkonoše Mts over a period of air pollution stress (1980–1995). Plant Ecol (143), 1–11. https://doi.org/10.1023/A:1009833313509

Valencia, S., Villegas, J.C., Hoyos, N., Duque-Villegas, M., Salazar, J.F. (2024): Streamflow response to land use/land cover change in the tropical Andes using multiple SWAT model variants. J Hydrol Reg (54), 101888. https://doi.org/10.1016/j.ejrh.2024.101888

Wang, H., Tetzlaff, D., Soulsby, C. (2018): Modelling the effects of land cover and climate change on soil water partitioning in a boreal headwater catchment. J Hydrol (558), 520–531. https://doi.org/10.1016/j.jhydrol.2018.02.002

Winkler, K., Fuchs, R., Rounsevell, M., Herold, M. (2021): Global land use changes are four times greater than previously estimated. Nat Comm (12), 2501. https://doi.org/10.1038/s41467-021-22702-2

Wojkowski, J., Walega, A., Radecki-Pawlik, A., Mlynski, D., Lepeška, T. (2022): The influence of land cover changes on landscape hydric potential and river flows: Upper Vistula, Western Carpathians. Catena (210), 105787. https://doi.org/10.1016/j.catena.2021.105878

Yang, J.L., Zhang, G.L. (2011): Water infiltration in urban soils and its effects on the quantity and quality of runoff. J Soils Sediments (11), 751–761. https://doi.org/10.1007/s11368-011-0356-1

Yu, X., Lamačová, A., Duffy, C., Krám, P., Hruška, J. (2016): Hydrological model uncertainty due to spatial evapotranspiration estimation methods. Comput Geosci (90), 90–101. https://doi.org/10.1016/j.cageo.2015.05.006

Zagajewski, B., Kluczek, M., Raczko, E., Njegovec, A., Dabija, A., Kycko, M. (2021): Comparison of Random Forest, Support Vector Machines, and Neural Networks for Post-Disaster Forest Species Mapping of the Krkonoše/Karkonosze Transboundary Biosphere Reserve. Remote Sens (13), 2581. https:// doi.org/10.3390/rs13132581

Zhu, Z., Woodcock, C.E. (2014): Automated cloud, cloud shadow, and snow detection in multitemporal Landsat data: An algorithm designed specifically for monitoring land cover change. Remote Sens Environ (152), 217-234. https://doi.org/10.1016/j.rse.2014.06.012.

Žoncová, M., Hronček, P., Gregorová, B. (2020): Mapping of the Land Cover Changes in High Mountains of Western Carpathians between 1990–2018: Case Study of the Low